Engineering Analysis with Boundary Elements 104 (2019) 1–7

Contents lists available at ScienceDirect

Engineering Analysis with Boundary Elements

journal homepage: www.elsevier.com/locate/enganabound

A meshless symplectic method for two-dimensional nonlinear Schrödinger equations based on radial basis function approximation☆

Zhengjie Sun[a,b]

[a] Department of Mathematics, Hong Kong Baptist University, Hong Kong
[b] School of Mathematical Sciences, Fudan University, Shanghai, PR China

ARTICLE INFO

MSC:
41A05
41A25
65D15
65N40

Keywords:
Conservative scheme
Schrödinger equation
Radial basis function
The method of lines

ABSTRACT

For two-dimensional nonlinear Schrödinger equations, we propose a meshless symplectic method based on radial basis function interpolation. With the method of lines, we first discretize the equation in spatial domain by using the radial basis function approximation method and obtain a finite-dimensional Hamiltonian system. Then appropriate time integrator is employed to derive the full-discrete symplectic scheme. Compared with the classical conservative methods that are only valid on uniform grids, our meshless method is conservative for both uniform grids and nonuniform nodes. The accuracy and conservation properties are analyzed in detail. Several numerical experiments are presented to demonstrate the accuracy and the conservation properties of our approach.

1. Introduction

The nonlinear Schrödinger (NLS) equation is the fundamental equation representing behavior of quantum mechanical systems and plays an important role in quantum mechanics. It appears in describing a wide range of physical phenomenon [11,13,17], such as plasma physics, nonlinear optic, electromagnetic wave propagation and self-focusing in laser pulses. The NLS equation is also a typical example of Hamiltonian PDEs which has several invariant quantities. In this paper, we consider the following nonlinear Schrödinger equation

$$i\psi_t + \psi_{xx} + \psi_{yy} + \alpha|\psi|^2\psi = 0,\ (x,y) \in \Omega \subset \mathbb{R}^2, t \in [0,T] \tag{1.1}$$

where $\psi(x, y, t)$ is a complex function, α is a real constant, $f : \mathbb{R} \to \mathbb{R}$ is a real function and $i^2 = -1$. Let $\psi(x,y,t) = u(x,y,t) + iv(x,y,t)$ with $u(x, y, t)$ and $v(x, y, t)$ are real functions, the Eq. (1.1) can be transformed into the following form

$$\begin{cases} u_t = -v_{xx} - v_{yy} - \alpha(u^2+v^2)v, \\ v_t = u_{xx} + u_{yy} + \alpha(u^2+v^2)u. \end{cases} \tag{1.2}$$

The above system can be comprised to an infinite-dimensional Hamiltonian system

$$\frac{d\mathbf{z}}{dt} = S\frac{\delta \mathcal{H}}{\delta \mathbf{z}}, \tag{1.3}$$

where $\mathbf{z} = (u, v)^T$, $S = \begin{pmatrix} 0 & 1 \\ -1 & 0 \end{pmatrix}$, $\frac{\delta \mathcal{H}}{\delta \mathbf{z}}$ is the variational derivative and the Hamiltonian functional is defined as

$$\mathcal{H} = \frac{1}{2}\int_\Omega \left[u_x^2 + u_y^2 + v_x^2 + v_y^2 - \frac{\alpha}{2}(u^2+v^2)^2\right]dxdy,$$

which is invariant with respect to time.

Under the appropriate boundary conditions, the Hamiltonian functional can be written as

$$\mathcal{H} = \frac{1}{2}\int_\Omega \left[-u\Delta u - v\Delta v - \frac{\alpha}{2}(u^2+v^2)^2\right]dxdy.$$

Moreover, the system (1.3) admits a constant symplectic structure

$$\omega = \int \mathbf{d}u \wedge \mathbf{d}v dxdy,$$

where $\wedge$ denotes the wedge product and $\mathbf{d}$ is the differential operator.

The standard method for obtaining the symplectic scheme for the NLS equation is the method of lines, which first discretizes the equation in space to derive a semi-discrete finite-dimensional Hamiltonian system and then employs an appropriate time integrator to get the final full-discrete symplectic scheme. Their are plenty of methods can be utilized in the spatial discretization including the finite difference method [3,6], the finite element method [34], discontinuous Galerkin method [29], Fourier pseudo-spectral method [5,7,8], wavelet collocation method [35,36] and so on.

☆ This work is supported by National Natural Science Foundation of China (11631015, 91330201) and Hong Kong Scholar Program 2018.
E-mail address: sunzhengjie1218@163.com

https://doi.org/10.1016/j.enganabound.2019.03.014
Received 25 October 2018; Received in revised form 31 January 2019; Accepted 11 March 2019
Available online 28 March 2019

However, the above methods for NLS equation require generating suitable meshes, which is time-consuming and difficult for high-dimensional problems with irregular domains. Thus there are some meshless methods for solving Schrödinger equation in the literature [1,21,22]. Furthermore, in [32], the authors proposed a meshless symplectic schemes for Hamiltonian partial differential equations based on radial basis function approximation. The prominent feature of the meshless method is that it can approximate multivariate function well even when the data are given on scattered nodes and thus is more efficient when compared with mesh-depended methods [4,30]. In addition to the radial basis function interpolation method [2,10,12,14,15], another meshless method called spectral meshless radial point interpolation method are also widely used in practical application to solve various types of problems [20,23–27].

Though the meshless symplectic method were shown to be powerful for solving linear equations including the multivariate Hamiltonian wave equation [32] and the two-dimensional Schrödinger equation [33], no positive results for nonlinear equations. Therefore, in this paper, we shall provide a meshless symplectic method for the nonlinear equation. Employing the method of lines, we first discretize the nonlinear equation in space with radial basis function interpolation to derive a semi-discrete finite-dimensional system, and analyze the conservation properties including the energy conservation and symplectic invariance. Then we adopt the Euler-centered scheme for temporal discretization and provide the error estimate.

The paper is organized as follows. In the next section, we introduce the radial basis function approximation method. Section 3 is devoted to our symplectic scheme for the NLS equation using the RBF collocation method and the Euler-centered scheme. This is followed by several numerical examples to corroborate our theoretical results. Finally, Section 5 contains some conclusions.

2. Radial basis function approximation method

Radial basis approximation method have been studied extensively in the past decades to approximate multivariate function. For details about radial basis function (RBF) method, one can refer to the monographs [4,9,30]. The good approximation properties and the ability to process scattered data make it be popular in applications. Especially, the radial basis interpolation method is successfully utilized for solving partial differential equations [14,15]. In the following, we give a brief introduction about radial basis function interpolation method.

Let $X = \{\mathbf{x}_j\}_{j=1}^N$ be the scattered sampling nodes and $\Phi_j(x) = \phi(\|x - x_j\|)$ be a radial function, where $\phi : \mathbb{R}^+ \to \mathbb{R}$ is a univariate function. A function f can be interpolated at X by

$$\mathcal{I}_X f = \sum_{j=1}^{N} c_j \phi(\|\mathbf{x} - \mathbf{x}_j\|), \mathbf{x} \in \mathbb{R}^d. \tag{2.1}$$

The coefficients c_j can be derived from the interpolation conditions $\mathcal{I}_X f|_X = f|_X$, namely

$$\mathbf{c} = \Phi^{-1}\mathbf{f},$$

where $\mathbf{c} = (c_1, \dots, c_N)^T, \Phi = (\phi(\|\mathbf{x}_\mathbf{k} - \mathbf{x}_j\|))$ and $\mathbf{f} = (f(x_1), \dots, f(x_N))^T$. Then the approximate function can be written as

$$\mathcal{I}_X f = (\phi(\|\mathbf{x} - \mathbf{x}_1\|), \dots, \phi(\|\mathbf{x} - \mathbf{x}_N\|))\Phi^{-1}\mathbf{f}.$$

To obtain the derivative approximation, we only need to apply the differential operator to the interpolant (2.1). If the Fourier transform of the radial basis function $\phi(x)$ satisfies $\hat{\phi}(\omega) \le o(1 + |\omega|)^{-K-d}$, then the interpolant $\mathcal{I}_X f$ possesses the following approximation order for the derivatives [30–32]

$$|(\mathcal{I}_X f)^{(\alpha)}(\mathbf{x}) - f^{(\alpha)}(\mathbf{x})| \le C h^{K/2-\alpha}, x \in \Omega, \tag{2.2}$$

where h is the fill distance defined by $h = \sup_{\mathbf{x}\in\Omega} \min_j \|\mathbf{x} - \mathbf{x}_j\|$.

3. The meshless symplectic method for the NLS equation

In this section, the radial basis function interpolation method will be used to construct the meshless symplectic scheme for the NLS equation. With the method of lines, we firstly discretize the continuous system in space to derive a semi-discrete finite-dimensional system. Then applying appropriate time integrators to derive the full-discrete scheme. The truncation error and the global error are also detailed analyzed.

3.1. Space discretization with radial basis function method

To discretize the NLW Eq. (1.2) in space, we let $\Phi(\mathbf{x}) = (\phi(\|\mathbf{x} - \mathbf{x}_1\|), \dots, \phi(\|\mathbf{x} - \mathbf{x}_N\|))$ $(\mathbf{x} = (x, y))$, and approximate the solution $u(\mathbf{x}, t), v(\mathbf{x}, t)$ by

$$\mathcal{I}_X u = \Phi(\mathbf{x})\Phi^{-1}U \sim u(\mathbf{x}, t)$$

and

$$\mathcal{I}_X v = \Phi(\mathbf{x})\Phi^{-1}V \sim v(\mathbf{x}, t)$$

respectively. Here $U = (u(\mathbf{x}_1, t), \dots, u(\mathbf{x}_N, t))^T$ and $V = (v(\mathbf{x}_1, t), \dots, v(\mathbf{x}_N, t))^T$.

The Laplacian Δu and Δv can be approximated by

$$\Delta\mathcal{I}_X u = (\Phi_{xx} + \Phi_{yy})(\mathbf{x})\Phi^{-1}U = \Delta\Phi(\mathbf{x})\Phi^{-1}U$$

and

$$\Delta\mathcal{I}_X v = (\Phi_{xx} + \Phi_{yy})(\mathbf{x})\Phi^{-1}V = \Delta\Phi(\mathbf{x})\Phi^{-1}V$$

respectively.

Then we use the radial basis function approximation together with a quadrature formula $\langle\cdot,\cdot\rangle_{\Phi^{-1}}$ to discretize the continuous Hamiltonian functional to get the discrete Hamiltonian functional

$$\begin{aligned}\mathcal{H}_d(U, V) = &-\frac{1}{2}\langle U, \Phi_\Delta\Phi^{-1}U\rangle_{\Phi^{-1}} - \frac{1}{2}\langle V, \Phi_\Delta\Phi^{-1}V\rangle_{\Phi^{-1}} \\ &- \frac{\alpha}{4}\langle \mathbf{1}, (U^2 + V^2)^2\rangle_{\Phi^{-1}},\end{aligned} \tag{3.1}$$

where $\Phi_\Delta = (\Delta\Phi(x_k - x_j))$, $(U^2 + V^2)^2 := (\dots, (u(\mathbf{x}_j)^2 + v(\mathbf{x}_j)^2)^2, \dots)^T$. The quadrature formula $\langle\cdot,\cdot\rangle_{\Phi^{-1}}$ was proposed in [32] and frequently used in [28,33].

According to the Hamiltonian form (1.3), we are required to calculate the discrete variational derivatives. From the definition of the finite-dimensional variational derivative, we have

$$\left\langle \frac{\delta H_d}{\delta U}, W \right\rangle_{\Phi^{-1}} = \frac{d}{d\epsilon}\bigg|_{\epsilon=0} \mathcal{H}_d(U + \epsilon W, V) = W^T \frac{\partial \mathcal{H}_d}{\partial U}, \ \forall W \in \mathbb{R}^N,$$

which gives us that

$$\frac{\delta \mathcal{H}_d}{\delta U} = \Phi\frac{\partial \mathcal{H}_d}{\partial U} = -\Phi_\Delta\Phi^{-1}U - \alpha\Phi\Lambda(U^2 + V^2)U,$$

where $\Lambda = \mathrm{diag}(\Lambda_j)$ with $\Lambda_j = \sum_k(\Phi^{-1})_{kj}$ and $(U^2 + V^2)U := (\dots, (u(\mathbf{x}_j)^2 + v(\mathbf{x}_j)^2)u(\mathbf{x}_j), \dots)^T$.

Similarly, we can obtain

$$\frac{\delta \mathcal{H}_d}{\delta V} = \Phi\frac{\partial \mathcal{H}_d}{\partial V} = -\Phi_\Delta\Phi^{-1}V - \alpha\Phi\Lambda(U^2 + V^2)V,$$

Thus we get the following semi-discrete system

$$\begin{cases} \frac{d}{dt}U = -\Phi_\Delta\Phi^{-1}V - \alpha\Phi\Lambda(U^2 + V^2)V, \\ \frac{d}{dt}V = \Phi_\Delta\Phi^{-1}U + \alpha\Phi\Lambda(U^2 + V^2)U. \end{cases} \tag{3.2}$$

The system (3.2) is indeed a finite-dimensional Hamiltonian system, namely

$$Z_t = J\nabla_Z\mathcal{H}_d,$$

where $Z = (U, V)^T$, $J = \begin{pmatrix} 0 & \Phi \\ -\Phi & 0 \end{pmatrix}$ is a skew-symmetric matrix.

The corresponding discrete symplectic form is given by

$$\omega_d = \mathbf{d}U \wedge \Phi^{-1}\mathbf{d}V. \tag{3.3}$$

Therefore we have the following conservation properties according to the classical Hamiltonian theory.

Theorem 3.1. *Let U, V be the solution of (3.2) and let $\mathcal{H}_d$, ω_d be defined as (3.1), (3.3) respectively, then the discrete Hamiltonian functional and the symplectic form are both conserved, namely*

$$\frac{d}{dt}\mathcal{H}_d = 0 \quad \text{and} \quad \frac{d}{dt}\omega_d = 0.$$

Next we shall prove that the semi-discrete Eq. (3.2) is an approximation to the continuous system. To start with, we give a result which has been proven in [32] about the approximation property of the inner product $\langle\cdot,\cdot\rangle_{\Phi^{-1}}$.

Lemma 3.1. *If $f, g \in L^1(\mathbb{R}^d)\bigcap L^2(\mathbb{R}^d)$ and $\int \hat{f}(w)w^\mu dw$, $\int \hat{g}(w)w^\mu dw$ exist for any $|\mu| \le s$, where μ is a multiple index and s is an integer. Suppose that the Fourier transform of the kernel function $\phi(x)$ satisfies*

$$\|\hat{\phi}(w) - 1\| \le \mathcal{O}(\|w\|^s), \text{ as } w \to 0,$$

then

$$\|F^T\Phi_\rho^{-1}G - \int f(\mathbf{x})g(\mathbf{x})d\mathbf{x}\|_\infty \le \mathcal{O}\left(h^{\frac{s^2}{2s+d}}\right),$$

where $F = (\dots, f(\mathbf{x}_j), \dots)^T$, $G = (\dots, g(\mathbf{x}_j), \dots)^T$ and $\Phi_\rho = (\frac{1}{\rho^d}\phi(\|\frac{\mathbf{x}_k - \mathbf{x}_j}{\rho}\|))$ with $\rho = h^{\frac{s}{2s+d}}$.

From this lemma, we observe that the discrete Hamiltonian functional $\mathcal{H}_d$ and discrete symplectic form ω_d are approximations to the continuous ones respectively by taking the new kernel function $\phi_\rho(\|\mathbf{x}\|) = \frac{1}{\rho^d}\phi(\|\frac{\mathbf{x}}{\rho}\|)$. Furthermore, we have the following theorem.

Theorem 3.2. *Under the assumptions of Lemma 3.1, the following estimate holds*

$$\begin{aligned}&\|\Phi_{\rho,\Delta}\Phi^{-1}U + \beta\Phi_\rho\Lambda(U^2+V^2)U - (\Delta U + \beta(U^2+V^2)U)\|_\infty \\ &\le \mathcal{O}\left(h^{K/2-2-\frac{4s}{2s+2}}\right) + \mathcal{O}\left(h^{\frac{s^2}{2s+2}}\right),\end{aligned}$$

where $\Phi_{\rho,\Delta} = (\Delta\phi_\rho(\|\mathbf{x}_k - \mathbf{x}_j\|))$.

Proof. According to (2.2), we obtain that

$$\|\Phi_{\rho,\Delta}\Phi^{-1}U - \Delta U\| \le \mathcal{O}\left(\frac{h^{K/2-2}}{\rho^4}\right) \le \mathcal{O}\left(h^{K/2-2-\frac{4s}{2s+2}}\right). \tag{3.4}$$

due to the fact that $\rho = h^{\frac{s}{2s+2}}$.

Then using the Lemma 3.2 in [28], we have

$$\|\Phi_\rho\Lambda - Id_N\|_\infty \le \mathcal{O}\left(h^{\frac{s^2}{2s+2}}\right), \tag{3.5}$$

where id_N is the N-dimensional identity operator.

Combining (3.4) and (3.5), we complete the proof. □

Up to now, we have obtained a semi-discrete finite-dimensional Hamiltonian system by using radial basis function approximation method and verified that the semi-discrete system is an approximation to the continuous one. Next we need to discretize the semi-discrete system in time to derive the full-discrete scheme.

3.2. Time discretization with the Euler-centered scheme

For the temporal discretization of the finite Hamiltonian system, there are various methods, such as generating function methods, high-order Runge–Kutta methods and composition methods [16,18,19]. Since our main contribution is on the spatial discretization, we only give a simple case here for illustration. We employ the Euler-centered scheme, which is a second-order implicit symplectic scheme.

Let $\hat{u}(\mathbf{x}_j, t^n)$, $\hat{v}(\mathbf{x}_j, t^n)$ be the approximations to $u(\mathbf{x}_j, t^n)$, $v(\mathbf{x}_j, t^n)$ respectively. Let τ be the time step and $t^n = t_0 + n\tau$. Denote $\hat{U}^n = (\hat{u}(\mathbf{x}_1, t^n), \dots, \hat{u}(\mathbf{x}_N, t^n))^T$, $\hat{V}^n = (\hat{v}(\mathbf{x}_1, t^n), \dots, \hat{v}(\mathbf{x}_N, t^n))^T$ and $\hat{U}^{n+1/2} = \frac{\hat{U}^{n+1}+\hat{U}^n}{2}$, we obtain the full-discrete symplectic scheme for the NLW equation

$$\begin{cases}\hat{U}^{n+1} = \hat{U}^n - \tau\Phi_{\rho,\Delta}\Phi_\rho^{-1}\hat{V}^{n+1/2} - \tau\alpha\Phi_\rho\Lambda\left[(\hat{U}^{n+1/2})^2 + (\hat{V}^{n+1/2})^2\right]\hat{V}^{n+1/2}, \\ \hat{V}^{n+1} = \hat{V}^n + \tau\Phi_{\rho,\Delta}\Phi_\rho^{-1}\hat{U}^{n+1/2} + \tau\alpha\Phi_\rho\Lambda\left[(U^{n+1/2})^2 + (\hat{V}^{n+1/2})^2\right]\hat{U}^{n+1/2}.\end{cases} \tag{3.6}$$

The system has a constant symplectic form $\omega_d^n = \mathbf{d}U^n \wedge \Phi_\rho^{-1}dV^n$.

Let $\hat{\Psi}^n = \hat{U}^n + i\hat{V}^n$, system (3.6) can be written as the following equivalent form

$$i\hat{\Psi}^{n+1} - i\hat{\Psi}^n + \tau\Phi_{\rho,\Delta}\Phi^{-1}\hat{\Psi}^{n+1/2} + \tau\alpha\Phi_\rho\Lambda(|\hat{\Psi}^{n+1/2}|^2)\hat{\Psi}^{n+1/2} = 0. \tag{3.7}$$

Define R^n as

$$R^n := i\Psi^{n+1} - i\Psi^n + \tau\Phi_{\rho,\Delta}\Phi_\rho^{-1}\Psi^{n+1/2} + \tau\alpha\Phi_\rho\Lambda(|\Psi^{n+1/2}|^2)\Psi^{n+1/2}, \tag{3.8}$$

where Ψ^n is the solution of Eq. (1.1) at time t_n. We can prove the estimates about the truncation error and the global error.

Theorem 3.3. *(Truncation error.) Assume that $u(\mathbf{x}, t) \in C^3(0, T; C^2(\Omega))$, $v(\mathbf{x}, t) \in C^3(0, T; C^2(\Omega))$. Let the truncation error bedefined as (3.8), then we have*

$$|R^n| \le \mathcal{O}(\tau^2 + h^p),$$

where $p = \min\{K/2 - 2 - \frac{4s}{2s+2}, \frac{s^2}{2s+2}\}$.

Proof. Based on Taylor expansion and the Theorem 3.2, we have

$$|\Psi^{n+1} - \Psi^n - \tau\Psi_t^{n+1/2}| \le \mathcal{O}(\tau^3)$$

and

$$\begin{aligned}&|\Phi_{\rho,\Delta}\Phi_\rho^{-1}\Psi^{n+1/2} + \alpha\Phi_\rho\Lambda(|\Psi^{n+1/2}|^2)\Psi^{n+1/2} \\ &\quad - \left(\Delta\Psi^{n+1/2} + \alpha(|\Psi^{n+1/2}|^2)\Psi^{n+1/2}\right)| \le \mathcal{O}\left(h^{K/2-2-\frac{4s}{2s+2}}\right) + \mathcal{O}\left(h^{\frac{s^2}{2s+2}}\right).\end{aligned}$$

Moreover, since Ψ^n is the solution of Eq. (1.1), we have

$$i\Psi_t^{n+1/2} + \Delta\Psi^{n+1/2} + \alpha(|\Psi^{n+1/2}|^2)\Psi^{n+1/2} = 0$$

and

$$|R^n| \le \mathcal{O}(\tau^2 + h^p).$$

□

Theorem 3.4. *(Global error.) Let Ψ^n, $\hat{\Psi}^n$ be the solutions of Eq. (1.1), (3.7) respectively. Denote $e^n = \Psi^n - \hat{\Psi}^n$, $p = \min\{K/2 - 2 - \frac{4s}{2s+2}, \frac{s^2}{2s+2}\}$. Then under the assumptions of Theorem 3.3, the following estimate holds*

$$\|e^L\|_{\Phi_\rho^{-1}} \le \mathcal{O}(\tau^2 + h^p), \ L = T/\tau.$$

Proof. Since $\hat{\Psi}^n$ satisfies

$$i\frac{\hat{\Psi}^{n+1} - \hat{\Psi}^n}{\tau} + \Phi_{\rho,\Delta}\Phi_\rho^{-1}\hat{\Psi}^{n+1/2} + \alpha\Phi_\rho\Lambda(|\hat{\Psi}^{n+1/2}|^2)\hat{\Psi}^{n+1/2} = 0, \tag{3.9}$$

we subtract (3.9) from (3.8) yields the following error equation

$$i\frac{e^{n+1} - e^n}{\tau} + \Phi_{\rho,\Delta}\Phi_\rho^{-1}e^{n+1/2} + \alpha g^{n+1/2} = R^n, \tag{3.10}$$

where

$$g^{n+1/2} = \Phi_\rho\Lambda\left[(|\Psi^{n+1/2}|^2)\Psi^{n+1/2} - (|\hat{\Psi}^{n+1/2}|^2)\hat{\Psi}^{n+1/2}\right].$$

Computing the inner product $\langle\cdot,\cdot\rangle_{\Phi_\rho^{-1}}$ of (3.10) with $e^{n+1/2}$ and taking the imaginary part, we have

$$\frac{1}{2\tau}\left(\|e^{n+1}\|_{\Phi_\rho^{-1}}^2 - \|e^n\|_{\Phi_\rho^{-1}}^2\right) + \mathrm{Im}\langle\alpha g^{n+1/2}, e^{n+1/2}\rangle_{\Phi_\rho^{-1}} = \mathrm{Im}\langle R^n, e^{n+1/2}\rangle_{\Phi_\rho^{-1}}. \tag{3.11}$$

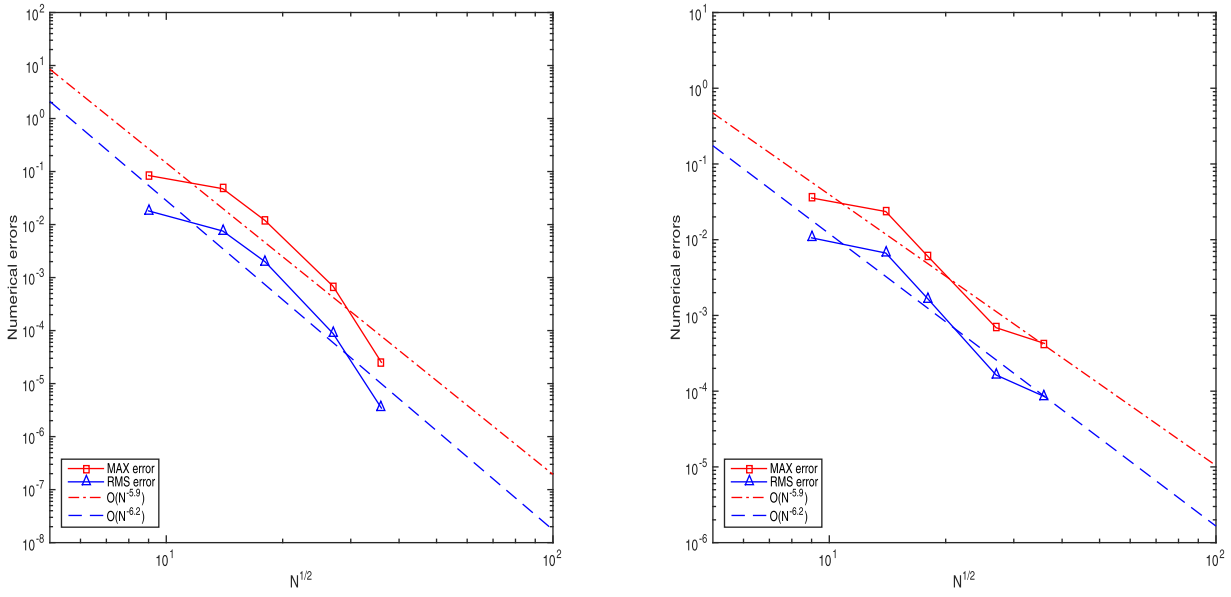

(a) Real part (b) Imaginary part

Fig. 1. The convergence results for numerical solution of Eq. (4.1).

To estimate $\|e^n\|_{\Phi_\rho^{-1}}$, we establish the following inequalities

$$\|g^{n+1/2}\|_{\Phi_\rho^{-1}} \le C\|e^{n+1/2}\|_{\Phi_\rho^{-1}},$$

$$\left|\left\langle \alpha g^{n+1/2}, e^{n+1/2}\right\rangle_{\Phi_\rho^{-1}}\right| \le C\left(\|e^n\|^2_{\Phi_\rho^{-1}} + \|e^{n+1}\|^2_{\Phi_\rho^{-1}}\right),$$

$$\left|\left\langle R^n, e^{n+1/2}\right\rangle_{\Phi_\rho^{-1}}\right| \le \frac{1}{2}\|R^n\|^2_{\Phi^{-1}} + \frac{1}{4}\left(\|e^n\|^2_{\Phi_\rho^{-1}} + \|e^{n+1}\|^2_{\Phi_\rho^{-1}}\right).$$

Therefore,

$$\frac{1}{2\tau}\left(\|e^{n+1}\|^2_{\Phi_\rho^{-1}} - \|e^n\|^2_{\Phi_\rho^{-1}}\right) \le C\left(\|e^n\|^2_{\Phi_\rho^{-1}} + \|e^{n+1}\|^2_{\Phi_\rho^{-1}}\right) + \frac{1}{2}\|R^n\|^2_{\Phi_\rho^{-1}}.$$

This together with Gronwall inequality gives that

$$\|e^L\|^2_{\Phi_\rho^{-1}} \le \left(\|e^0\|^2_{\Phi_H^{-1}} + \tau\sum_{k=1}^{L}\|R^k\|^2_{\Phi_\rho^{-1}}\right)e^{4CT},\ L = T/\tau.$$

Since

$$\|e^0\|^2_{\Phi_\rho^{-1}} = 0,\ \|R^k\|_{\Phi_\rho^{-1}} \le \mathcal{O}(\tau^2 + h^p),$$

we then obtain the desired error estimate

$$\|e^L\|_{\Phi_\rho^{-1}} \le \mathcal{O}(\tau^2 + h^p).$$

□

4. Numerical examples

In this section, several examples are presented to demonstrate the good accuracy and the conservation properties of our method.

Example 1. We first consider a linear Schrödinger equation

$$i\psi_t + \psi_{xx} + \psi_{yy} + w(x,y)\psi = 0, \tag{4.1}$$

with the Dirichlet boundary conditions and the potential function given by $w(x,y) = 3 - 2\tanh^2 x - 2\tanh^2 y$. The exact solution is

$$\psi(x,y,t) = \frac{ie^{it}}{\cosh x \cosh y}. \tag{4.2}$$

The problem is solved on a circular domain $x^2 + y^2 \le 25$ with the time step $\tau = 0.001$ till time $T = 1$. We employ the Halton points limited in the circle as the scattered nodes and adopt the inverse multiquadric (IMQ) kernel $\phi(x) = \frac{1}{\sqrt{1+(er)^2}}$ in radial basis approximation with a shape parameter $e = 1$. Numerical results of maximum errors and the root mean square (RMS) errors for real part and imaginary part are presented in Fig. 1. The definition of RMS error can be found in many references, for example [21,32]. Fig. 2 shows the graphs of numerical solution for real part and imaginary part at time $T = 1$ on circular domain. Figs. 1 and 2 both demonstrate that the proposed method possesses a high order of convergence.

Table 1
Numerical results with uniform points and shape parameter $e = 0.61$ by using our method.

$N\times N$	L^2-error	order	L^∞-error	order
10×10	1.6691e−2		5.8054e−3	
15×15	3.6130e−3	3.77	1.2745e−3	3.74
20×20	8.7220e−4	4.94	3.2816e−4	4.72
25×25	2.6971e−4	5.26	8.9240e−5	5.84

Example 2. Consider the two dimensional nonlinear cubic Schrödinger equation with periodic boundary conditions

$$i\psi_t + \psi_{xx} + \psi_{yy} + \alpha|\psi|^2\psi = 0. \tag{4.3}$$

A progressive plane wave solution is given by [35]

$$\psi(x,y,t) = A\exp(i(c_1x + c_2y - \beta t)), \tag{4.4}$$

where $\beta = c_1^2 + c^2 - \alpha|A|^2$, A, c_1, c_2 are constants.

For accuracy test, the problem is solved on spatial domain $[0, 2\pi]^2$ till time $T = 1$ by taking $A = 1$, $c_1 = c_2 = 1$, $\alpha = 1$. In order to estimate the approximation order in spatial domain, a small time step $\tau = 0.001$ is chosen. We use radial basis function interpolation with IMQ in spatial discretization, where e is the shape parameter. The L^2, L^∞ errors and the convergence orders by using our method with uniform grids are given in Table 1, while the results with irregularly spaced Halton points [9] are presented in Table 2. The convergence order is calculated by the formula $\frac{\ln(Err_1/Err_2)}{\ln(h_1/h_2)}$, where h_j, Err_j, $(j = 1, 2)$ are spatial step size and the error with step size $h_j = \frac{2\pi}{N}$, respectively.

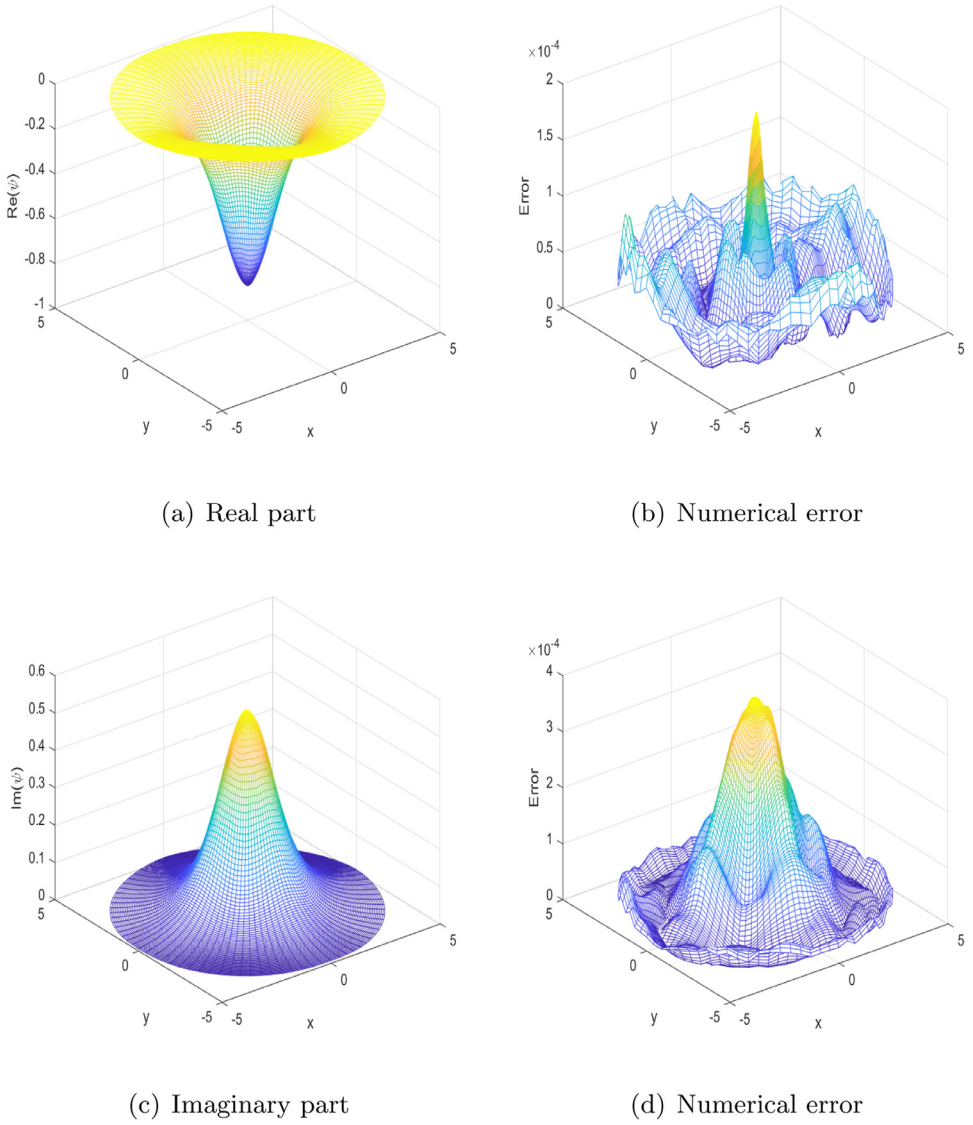

(a) Real part (b) Numerical error

(c) Imaginary part (d) Numerical error

Fig. 2. Graphs of numerical solution and absolute error for real and imaginary part at $T = 1$ on circular domain.

Table 2
Numerical results with Halton points and shape parameter $e = 0.56$ by using our method.

$N \times N$	L^2-error	order	L^∞-error	order
10×10	1.4687e−1		4.9242e−2	
15×15	4.7863e−2	2.77	1.4167e−2	3.07
20×20	1.4062e−2	4.26	4.2826e−3	4.16
25×25	4.5986e−3	5.01	1.3637e−3	5.13

Remark 4.1. From Tables 1 and 2, we can observe that whether for uniform or scattered nodes, our method has good accuracy.

Example 3. Consider the same example as Example 1. In this example, we will turn to the long time simulation. We solve the Eq. (4.3) on square domain $[0, 2\pi]^2$ till time $T = 10$ using our approach with IMQ kernel, $\tau = 0.001$ and $N = 32$. The numerical errors at different terminal times are shown in Table 3 for uniform points, and Table 4 for Halton points respectively.

Remark 4.2. From Tables 3 and 4, we see that the numerical errors does not increase rapidly as time evolves, which demonstrates that our scheme is stable and suitable for long time simulation.

Table 3
Numerical errors with uniform points at different times.

Times	L^2-error	L^∞-error
2	1.3076e−3	3.9172e−4
4	1.8712e−3	5.9626e−4
6	2.0805e−3	7.8293e−4
8	1.4510e−3	6.8797e−4
10	3.9705e−3	1.8522e−3

Table 4
Numerical errors with Halton points at different times.

Times	L^2-error	L^∞-error
2	1.5636e−2	4.0617e−3
4	2.6437e−2	1.0856e−2
6	3.0871e−2	1.4129e−2
8	3.8230e−2	1.6093e−2
10	2.8029e−2	1.1979e−2

Finally, we focus on the conservation of energy. The problem is considered till time $T = 10$ with $\tau = 0.001$ and $N = 32$ as above. Fig. 3 shows the variations of discrete energy error at different times with uniform points and Halton points by using the proposed method. The discrete

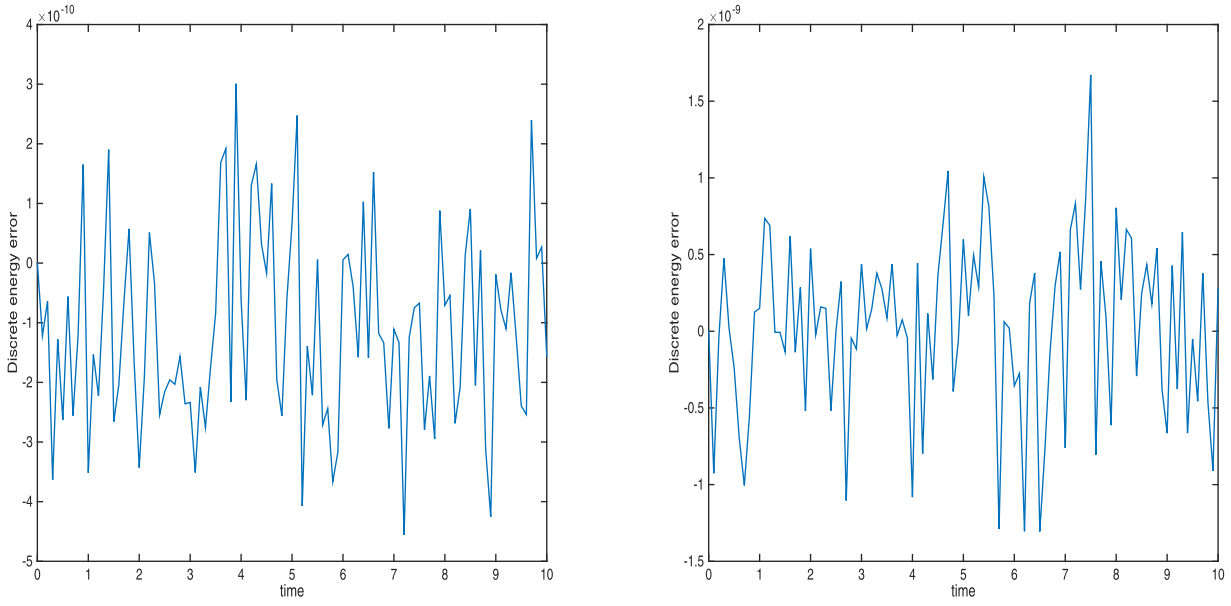

(a) Uniform Points (b) Halton Points

Fig. 3. The variation of discrete energy errors by using our method on uniform points and Halton points.

energy errors are measured by $Err_{\mathcal{H}}^n = \mathcal{H}_d^n - \mathcal{H}_d^0$, where $\mathcal{H}_d^n$, $\mathcal{H}_d^0$ are the discrete energy at time t_n and t_0 respectively.

Remark 4.3. Fig. 3 vividly shows that our approach conserves the energy well whether for uniform or scattered points. However, as we know, the general conservative schemes for Schrödinger equations can not be employed to scattered nodes [5], which demonstrates the superiority of our method.

5. Conclusions

A meshless conservative method based on radial basis approximation is proposed for solving two-dimensional nonlinear Schrödinger equations. Using the radial basis function approximation method, we discretize the equation in space to obtain the semi-discrete system. Then the Euler-centered scheme is employed to derive the full-discrete system. The error estimates including the accuracy of the our approach, the truncation error and the global error of full-discrete scheme are presented in the paper. The theoretical analysis and numerical results both show that our method has high-order accuracy and can conserve the energy whether for uniform or scattered nodes. The proposed method can be generalized to solve other Hamiltonian PDEs with conservation properties.

References

[1] Abbasbandy S, Ghehsareh HR, Hashim I. A meshfree method for the solution of two-dimensional cubic nonlinear Schrödinger equation. Eng Anal Bound Elem 2013;37(6):885–98.
[2] Abbasbandy S, Ghehsareh HR, Hashim I, Alsaedi A. A comparison study of meshfree techniques for solving the two-dimensional linear hyperbolic telegraph equation. Eng Anal Bound Elem 2014;47:10–20.
[3] Aydin A, Karasözen B. Symplectic and multi-symplectic methods for coupled nonlinear Schrödinger equations with periodic solutions. Comput Phys Commun 2007;177:566–83.
[4] Buhmann MD. Radial basis functions: theory and implementations. Cambridge University Press; 2003.
[5] Cai JX, Wang YS. A conservative fourier pseudospectral algorithm for a coupled nonlinear schrödinger system. Chin Phys B 2013;22:060207.
[6] Celledoni E, Grimm V, McLachlan RI, McLaren DI, O'Neale D, Owren B, Quispel GRW. Preserving energy resp. dissipation in numerical PDEs using the "Average Vector Field" method. J Comput Phys 2012;231:6770–89.
[7] Chen JB, Qin MZ. Multi-symplectic Fourier pseudospectral method for the nonlinear Schrödinger equation. Electr Trans Numer Anal 2001;12:193–204.
[8] Chen YM, Song SH, Zhu HJ. The multi-symplectic Fourier pseudospectral method for solving two-dimensional Hamiltonian pdes. J Comput Appl Math 2011;236:1354–69.
[9] Fasshauer GE. Meshfree approximation methods with MATLAB. World Scientific Publishing Co. Pte. Ltd; 2007.
[10] Franke C, Schaback R. Solving partial differential equations by collocation using radial basis functions. Appl Math Comput 1998;93(1):73–82.
[11] Griffiths DJ. Introduction to quantum mechanics. New Jersey: Prentice Hall; 1995.
[12] Hajiketabi M, Abbasbandy S. The combination of meshless method based on radial basis functions with a geometric numerical integration method for solving partial differential equations: application to the heat equation. Eng Anal Bound Elem 2018;87:36–46.
[13] Hasegawa A. Optical solitons in fibers. Berlin: Springer; 1989.
[14] Kansa EJ. Multiquadrics-a scattered data approximation scheme with application to computational fluid dynamics i. surface approximation and partial derivative estimates. Comput Math Appl 1990;19:127–45.
[15] Kansa EJ. Multiquadrics-a scattered data approximation scheme with application to computational fluid dynamics ii. solutions to parabolic, hyperbolic and elliptic partial differential equations. Comput Math Appl 1990;19:147–61.
[16] Kong LH, Liu RX, Zheng XH. A survey on symplectic and multi-symplectic algorithms. Appl Math Comput 2007;186:670–84.
[17] Levy M. Parabolic equation methods for electromagnetic wave propagation. IEEE electromagnetic waves series, 45. England: Padstow: IET; 2000.
[18] McLachlan RI. Symplectic integration of Hamiltonian wave equations. Numer Math 1994;66:465–92.
[19] Sanz-Serna JM, Calvo MP. Numerical Hamiltonian problems. London: Chapman & Hall; 1994.
[20] Shivanian E, Aslefallah M. Stability and convergence of spectral radial point interpolation method locally applied on two-dimensional pseudoparabolic equation. Numer Methods Partial Differ Equ 2017;33(3):724–41.
[21] Shivanian E, Jafarabadi A. An efficient numerical technique for solution of two-dimensional cubic nonlinear Schrödinger equation with error analysis. Eng Anal Bound Elem 2017;83:74–86.
[22] Shivanian E, Jafarabadi A. Error and stability analysis of numerical solution for the time fractional nonlinear Schrödinger equation on scattered data of general-shaped domains. Numer Methods Partial Differ Equ 2017;33(4):1043–69.
[23] Shivanian E, Jafarabadi A. Inverse Cauchy problem of annulus domains in the framework of spectral meshless radial point interpolation. Eng Comput 2017;33(3):431–42.
[24] Shivanian E, Jafarabadi A. Numerical solution of two-dimensional inverse force function in the wave equation with nonlocal boundary conditions. Inverse Prob Sci Eng 2017;25(12):1743–67.
[25] Shivanian E, Jafarabadi A. An inverse problem of identifying the control function in two and three-dimensional parabolic equations through the spectral meshless radial point interpolation. Appl Math Comput 2018;325:82–101.
[26] Shivanian E, Jafarabadi A. The numerical solution for the time-fractional inverse problem of diffusion equation. Eng Anal Bound Elem 2018;91:50–9.
[27] Shivanian E, Jafarabadi A. The spectral meshless radial point interpolation method for solving an inverse source problem of the time-fractional diffusion equation. Appl Numer Math 2018;129:1–25.

[28] Sun ZJ, Wu ZM. Meshless conservative scheme for nonlinear Hamiltonian partial differential equations. J Sci Comput 2018;76:1168–87.
[29] Tang WS, Sun YJ, Cai WJ. Discontinuous Galerkin methods for Hamiltonian ODEs and PDEs. J Comput Phys 2017;330:340–64.
[30] Wendland H. Scattered data approximation. Cambridge Monographs on Applied and Computational Mathematics. Cambridge: Cambridge University Press; 2004.
[31] Wu ZM, Liu JP. Generalized strang-fix condition for scattered data quasi-interpolation. Adv Comput Math 2005;23:201–14.
[32] Wu ZM, Zhang SL. A meshless symplectic algorithm for multi-variate Hamiltonian PDEs with radial basis approximation. Eng Anal Bound Elem 2015;50:258–64.
[33] Zhang SL, Chen SY. A meshless symplectic method for two-dimensional Schrödinger equation with radial basis functions. Comput Math Appl 2016;72:2143–50.
[34] Zhen L, Bai Y, Wu K. Symplectic and multi-symplectic schemes with finite element methods. Phys. Lett. A 2003;314:443–55.
[35] Zhu HJ, Chen YM, Song SH, Hu HY. Symplectic and multi-symplectic wavelet collocation methods for two-dimensional Schrödinger equations. Appl Numer Math 2011;61:308–21.
[36] Zhu HJ, Song SH, Tang YF. Multi-symplectic wavelet collocation method for the nonlinear Schrödinger equation and the camassa-holm equation. Comput Phys Commun 2011;182:616–27.